# Faraday rotation measures of Northern hemisphere pulsars using CHIME/Pulsar

C. Ng [1]⋆ A. Pandhi,[2] A. Naidu,[3,4] E. Fonseca,[3,4] V. M. Kaspi,[3,4] K. W. Masui,[5,6]
R. Mckinven,[1,2] A. Renard,[1] P. Scholz,[1,7] I. H. Stairs,[8] S. P. Tendulkar[3,4]
and K. Vanderlinde[1,2]

[1]*Dunlap Institute for Astronomy and Astrophysics, University of Toronto, 50 St. George Street, Toronto, ON M5S 3H4, Canada*
[2]*David A. Dunlap Institute Department of Astronomy & Astrophysics, University of Toronto, 50 St. George Street, Toronto, ON M5S 3H4, Canada*
[3]*Department of Physics, McGill University, 3600 rue University, Montréal, QC H3A 2T8, Canada*
[4]*McGill Space Institute, McGill University, 3550 rue University, Montréal, QC H3A 2A7, Canada*
[5]*MIT Kavli Institute for Astrophysics and Space Research, Massachusetts Institute of Technology, 77 Massachusetts Ave, Cambridge, MA 02139, USA*
[6]*Department of Physics, Massachusetts Institute of Technology, 77 Massachusetts Ave, Cambridge, MA 02139, USA*
[7]*Dominion Radio Astrophysical Observatory, Herzberg Astronomy & Astrophysics Research Centre, National Research Council Canada, PO Box 248, Penticton, V2A 6J9, Canada*
[8]*Department of Physics and Astronomy, University of British Columbia, 6224 Agricultural Road, Vancouver, BC V6T 1Z1, Canada*

## ABSTRACT

Using commissioning data from the first year of operation of the Canadian Hydrogen Intensity Mapping Experiment's (CHIME) Pulsar backend system, we conduct a systematic analysis of the Faraday Rotation Measure (RM) of the Northern hemisphere pulsars detected by CHIME. We present 55 new RMs as well as obtain improved RM uncertainties for 25 further pulsars. CHIME's low observing frequency and wide bandwidth between 400 and 800 MHz contribute to the precision of our measurements, whereas the high cadence observation provides extremely high signal-to-noise co-added data. Our results represent a significant increase of the pulsar RM census, particularly regarding the Northern hemisphere. These new RMs are for sources that are located in the Galactic plane out to 10 kpc, as well as off the plane to a scale height of ∼16 kpc. This improved knowledge of the Faraday sky will contribute to future Galactic large-scale magnetic structure and ionosphere modelling.

**Key words:** techniques: polarimetric – pulsars: general – ISM: magnetic fields.

## 1 INTRODUCTION

Radio pulsars have emission that is among the most polarized of all astronomical sources. As the linearly polarized emission travels through the interstellar medium (ISM) in the presence of magnetic fields, free electrons along the line of sight (LOS) lead to Faraday rotation of the observed pulsar radio emission. The differential of Faraday rotation (or the change in polarization angle, $\Delta$PA) between two observing frequencies is associated with the Rotation Measure (RM) and the observing wavelength ($\lambda$):

$$\Delta\text{PA} = \text{RM}\lambda^2. \tag{1}$$

RM is in turn related to the number density of the free electrons along the LOS and the magnetic field of the LOS plasma ($B$) by:

$$\text{RM} = 0.812 \,\text{rad m}^{-2} \int_0^d \left[\frac{n_e(s)}{\text{cm}^{-3}}\right] \left[\frac{B(s)}{\mu G}\right] \cdot \left(\frac{ds}{\text{pc}}\right), \tag{2}$$

where $d$ is the distance to the pulsar. At the same time, the pulsar emission is dispersed by the plasma electrons. The ratio of the RM to the dispersion measure (DM) provides an estimate of the integrated magnetic field strength along the parallel LOS:

$$\langle B_{\parallel} \rangle = 1.232 \,\mu G \left(\frac{\text{RM}}{\text{rad m}^{-2}}\right) \left(\frac{\text{DM}}{\text{pc cm}^{-3}}\right)^{-1}. \tag{3}$$

The Faraday rotation of pulsars is thus a powerful tool for studying the Galactic magnetic field (GMF). The study of magnetic field structure is important as it plays a critical role in numerous astrophysical processes, see for example, a review by Noutsos (2012). Currently in the *ATNF Pulsar Catalogue*[1] (V1.61; Manchester et al. 2005), there are 1167 pulsars with a published RM, which is approximately 42 per cent of the full pulsar population. These pulsars are distributed throughout the Galactic disc, mapping the $< B_{\parallel} >$ of over a thousand LOS. Numerous previous studies

⋆ E-mail: cherrywyng@gmail.com

[1]http://www.atnf.csiro.au/research/pulsar/psrcat

have used pulsar RMs to model the large-scale component of the GMF (Noutsos et al. 2015; Han et al. 2018; Sobey et al. 2019). Pulsar RMs can also be combined with extragalactic RMs for a more comprehensive view of the Galactic disc and halo (e.g. Van Eck et al. 2011).

There is room for improvement in using pulsar RMs to model the GMF. Currently, a large fraction of the available pulsar RMs is located near the Galactic plane and is concentrated within a few kiloparsec from the Sun. Most of the previously measured RMs were obtained with the Australian Parkes telescope in the Southern hemisphere which operates at 1.4 GHz. Since Faraday rotation depends on wavelength squared (equation 1), lower frequency observations lead to more precise measurements of RMs. Multiple aperture array telescopes at low frequency have come online in recent years. They will be providing an enhanced view of the polarized sky. These facilities include the Low-Frequency Array (LOFAR; van Haarlem et al. 2013), the Long-Wavelength Array (LWA; Taylor et al. 2012), and the Murchison Widefield Array (MWA; Tingay et al. 2013; Wayth et al. 2018). Most recently, the Canadian Hydrogen Intensity Mapping Experiment (CHIME; CHIME/FRB Collaboration 2018), which is a dense-packed interferometer operating at 400–800 MHz, has also begun commissioning observations.

In this paper, we present a study of pulsar RMs using CHIME data. An overview of the telescope and observational data is provided in Section 2 and the method of analysis is detailed in Section 3. We report on our results in Section 4, including 55 new RMs as well as improvement in the uncertainties of 25 catalogue RM values. In Section 5, we discuss the implications of our work and conclude in Section 6.

## 2 TELESCOPE OVERVIEW AND OBSERVATIONS

### 2.1 The CHIME/Pulsar backend

CHIME is a radio telescope hosted by the Dominion Radio Astrophysical Observatory (DRAO) in British Columbia, Canada. CHIME operates across a wide bandwidth of 400–800 MHz and has a collecting area ($\sim 80 \times 100\,\text{m}^2$) and point-source sensitivity comparable to that of other 100-m class radio telescopes. The reflecting surface of CHIME consists of four parabolic cylinders. It is a transit telescope with no moving parts. For the CHIME/Pulsar project, we combine the signals from the 1024 dual polarization feeds and form 10 tied-array beams that are available as raw voltages (Ng 2018). This means that we can track 10 different pulsars at any given time as they transit through CHIME's field of view, along the meridian. This provides very high-cadence scheduling: while many of the Northern hemisphere pulsars are being monitored daily, the longest cadence to cycle through all sources in the northern sky is only $\sim$10 d. This is reflected in the long co-added integration length of our data (Total$_{\text{fold}}$) and the high signal to noise (S/N) achieved as listed in Table A1. The transit time of each source is a function of the declination; transit times can range from tens of minutes to hours for circumpolar sources. CHIME can in principle observe down to a declination of $-20°$.

### 2.2 Observations and data types

The beam-formed baseband data of the CHIME/Pulsar backend are dual-polarization, complex-sampled, and split into 1024 frequency channels with eight bits per complex sample. For each observing scan, we generate 'fold mode' archives using the 'Digital Signal Processing for Pulsars' (dspsr) suite, an open source GPU-based library developed by van Straten & Bailes (2011). These data are coherently dedispersed at the known DM (taken from the *ATNF* catalogue) and then folded at the catalogue spin period with nominally 256 phase bins at 10-s sub-integration and the four Stokes (*I*, *Q*, *U*, and *V*) parameters are recorded. While 256 phase bins should be adequate for most of the pulsars studied in this work, we note that using too few phase bins could potentially lead to depolarization. A number of our pulsar observations were recorded with up to 2048 phase bins. For these sources, we step through the range of 32–2048 phase bins and see no obvious trend in the resulting RMs that is greater than their uncertainties.

The data have not yet been polarization calibrated. The beam shape of any aperture array is complicated, especially in the case of CHIME where over a thousand analog input components are involved. A proper calibration will be implemented in the near future. Fortunately, Faraday rotation is generally unaffected because there are no wavelength-squared dependencies in the beam shape. We have verified our RM analysis pipeline by cross-checking with 100 pulsars with catalogue RMs and obtained consistent results for most of them (see Section 4.1). We note that uncalibrated data could potentially show instrumental polarization, where emission from Stokes *I* contaminates the other Stokes parameters. This is manifested as a peak in the Faraday spectrum centred at zero; see, for example PSRs J0026+6320, J0324+5239, B0331+45, and J0426+4933 in Fig C1. For a discrete sampled Faraday dispersion function, the Full Width Half Maximum (FWHM) of the theoretical RM spread function (RMSF) is given by $\delta\phi = 3.8/\Delta(\lambda^2)$ (Brentjens & de Bruyn 2005). For CHIME, we have a $\delta\phi$ of about 9 rad m$^{-2}$. The majority of our RM values have a higher magnitude than this, so the presence of leakage does not cause any confusion. However, this could have an effect on small RMs and is further discussed in Section 4.2.

## 3 DATA REDUCTION AND ANALYSIS

Our offline data analysis pipeline is heavily based on modules from the PSRCHIVE pulsar data processing (Hotan, van Straten & Manchester 2004; van Straten, Demorest & Oslowski 2012). First, data affected by radio frequency interference are excised by identifying outlier intensity values both in time and frequency. These sub-integrations and frequency channels are set to zero using paz and pazi. We create updated pulsar ephemerides using the TEMPO2 software package (Hobbs, Edwards & Manchester 2006) and we fit for DM using pdmp in order to properly co-add all available fold mode data to obtain the highest possible S/N. The S/N-optimized DM for each pulsar is listed as DM$_{\text{obs}}$ in Table A1. We have not taken into account any temporal DM variations in this work. DM variations up to the order of $10^{-2}\,\text{cm}^{-3}\text{pc/yr}$ have been reported in the literature (see e.g. Lam et al. 2015). We have verified that offsetting the folding DM by this amount does not lead to difference in RM greater than the RM uncertainty quoted here.

We quantify the RM of these co-added data using the rmfit[2] tool. An initial guess of the RM is found by brute force searching the RM range of $\pm 1500\,\text{rad m}^{-2}$. At each trial RM, rmfit corrects for the associated Faraday rotation and computes the total linear polarization $L = (Q^2 + U^2)^{1/2}$ across the on-pulse region. rmfit then fits a Gaussian to the resultant RM spectrum to identify a peak RM. This RM value is then iteratively refined as follows: the data

---

[2]http://psrchive.sourceforge.net/manuals/rmfit/

are split in two equal frequency bands where each data segment is integrated and then compared to compute a weighted differential $\Delta$PA. The uncertainty of $\Delta$PA is minimized to obtain the best-fitting RM value. Previous studies such as Morello et al. (2020) have shown that the iterative method of rmfit can sometimes underestimate the RM uncertainty. For pulsars that have high enough S/N for RM to be obtained on a per-session basis (i.e. without having to co-add across multiple days), we use the spread of 1 standard deviation of these daily RM values as our uncertainty. This applies to 39 out of the 80 updated RMs reported in this work. For the remaining pulsars that are too weak to obtain per-session RM, we adopt the RM uncertainty given by the brute-force method of rmfit on the co-added data, which is conservatively calculated to be the range where the Gaussian fit for the RM spectrum drops by $2\sigma$.

Unmodelled profile evolution could lead to the addition of sine waves with amplitudes that have different frequency dependence and potentially introducing bias in the RM measurement. Profile evolution is expected to be most rapid at lower observing frequencies below 200 MHz (see e.g. Phillips & Wolszczan 1992). Upon a visual inspection, we do not see substantial variations among the pulsars in this sample and so have not attempted to fit for two-dimensional pulse profiles. The effect of ionospheric Faraday rotation has not been corrected in this work. To do that properly requires a careful modelling of the ionosphere and is out of scope for this project. However, all the observations on which this paper is based were obtained during the current minimum of solar activity. We estimate that ionospheric RM was usually less than 1 rad m$^{-2}$ and no more than $+2$ rad m$^{-2}$ even during daytime (Mevius 2018a,b).

## 4 RESULTS

### 4.1 Comparison to catalogue RMs

The data set used in this work is from the first year of CHIME/Pulsar commissioning observations, which spans 2018 September to 2019. In order to verify our RM pipeline and the CHIME data, we first attempt to cross-check RMs for pulsars that have a catalogue RM value. We analyse all pulsars above declination $\delta = 0°$ detected by CHIME that have a published RM between $\pm100$ rad m$^{-2}$. We detect unambiguous RMs in 100 pulsars and use them as our verification sample. As can be seen from Fig. 1, most of our observed RM (RM$_{obs}$) agree with the catalogue value (RM$_{cat}$), which is reassuring. In addition, we measure RMs with substantially lower uncertainties than those in the *ATNF* pulsar catalogue (V1.61) for 25 pulsars. This is likely due to the higher precision RM made possible from our lower frequency and large bandwidth observations, as well as the high S/N profiles, which result from long-duration co-added data.

Eight of the RMs we measure differ significantly from their catalogue values. These sources are annotated in Fig. 1. The catalogue RMs of three of those, namely PSRs J0538+2817, J0546+2441, and J0751+1807, are close to zero, which suggests that previous studies might have been contaminated by spectral leakage. We find that the RMs of four pulsars have changed by a few to a few tens of RM units in the time between their catalogue measurement epochs and our more recent CHIME detections. These include PSR B0144+59 with RM$_{cat}$ = $-19(4)$ rad m$^{-2}$ (Rand & Lyne 1994) compared to RM$_{obs}$ = $-9.5(5)$ rad m$^{-2}$, PSR B1612+07 with RM$_{cat}$ = $40(4)$ rad m$^{-2}$ (Hamilton & Lyne 1987) compared to RM$_{obs}$ = $28(3)$ rad m$^{-2}$, PSR B2148+52 with RM$_{cat}$ = $-44(11)$ rad m$^{-2}$ (Mitra et al. 2003) compared to RM$_{obs}$ = $-19.0(8)$ rad m$^{-2}$, and PSR J2240+5832 with RM$_{cat}$ = $24(4)$ rad m$^{-2}$ (Theureau et al. 2011) compared to RM$_{obs}$ = $17.1(11)$ rad m$^{-2}$. These differences
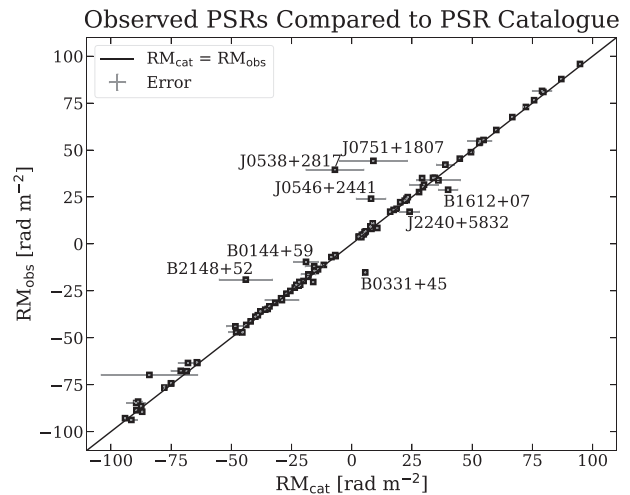


**Figure 1.** A comparison between RM$_{obs}$ and RM$_{cat}$ for 100 pulsars above $\delta = 0°$ detected by CHIME. The black line corresponds to the RM$_{obs}$ = RM$_{cat}$ trend, which we expect to see. PSRs B0144+59, B0331+45, J0538+2817, J0546+2441, J0751+1807, B1612+07, B2148+52, and J2240+5832 are highlighted as they significantly deviate from the RM$_{obs}$ = RM$_{cat}$ trend; these eight pulsars are discussed further in the main text.

are too big to be explained by any ionospheric corrections. It is possible that we are seeing a genuine temporal evolution of these RMs over the years, although there are no other data points in the literature to help verify this. The presence of an unusual local environment [e.g. the Supernova Remnant of Vela (Johnston et al. 2005), an eclipsing black widow binary (Breton et al. 2013)] has been suggested to cause a change in temporal RM, although these scenarios do not seem to apply to the four pulsars listed above. Finally, for PSR B0331+45, we obtain an RM$_{obs}$ of $-15.2(11)$ rad m$^{-2}$, which is discrepant with the latest result from Sobey et al. (2019) at $5.60(9)$ rad m$^{-2}$. Even though our data of PSR B0331+45 are affected by instrumental leakage, which shows up as a peak near zero in the RM spectrum (see Fig. C1), we detect a clear non-zero RM and the signal is confirmed upon inspecting the expected oscillation in Stokes $Q$. Given that our work and that of Sobey et al. (2019) are taken relatively close in time, it seems unlikely that the RM could have changed so much within a year or so. We note that there is an older published RM of this pulsar at $-41(20)$ rad m$^{-2}$ by Rand & Lyne (1994), which is consistent with our observed value.

### 4.2 New RMs for 55 pulsars

Over 500 known pulsars were detected by CHIME/Pulsar above $\delta = -20°$ in the first year of commissioning. We have sufficiently high S/N data for RM measurement for 109 of these pulsars that do not already have published RM values. We obtain new RMs for 55 of these pulsars; see Table A1 for details, and Figs C1–C3 for the individual RM spectra. We are not able to quantify RMs for the remaining pulsars because of two reasons: (1) instrumental leakage dominates 30 of those, which could potentially be improved when a polarization calibration scheme is carried out on CHIME data in the future; (2) no RM peak is detected in 24 pulsars, which could be because these pulsars are intrinsically weakly polarized. Refer to Appendix C for a list of these pulsars.

Thirteen of these 55 pulsars were already studied using LOFAR in Sobey et al. (2019), although they did not detect any significant RM

at the time (refer to table 2 in that publication). This may be because LOFAR's frequency channel widths are sufficiently broad that they lose >50 per cent sensitivity for $|RM|$ >163 rad m$^{-2}$, whereas for CHIME/Pulsar, with our frequency resolution of 390 kHz, we maintain full sensitivity out to an RM of roughly 1000 rad m$^{-2}$. Some of these pulsars lie along the Galactic plane, and LOFAR could be suffering from more scattering and depolarization at the high DM and RM due to its low-observing frequency. We note that there is likely some degree of profile scattering for some of the pulsars in the CHIME band as well. We have not attempted to model the effect of scattering on RM here; the difference is expected to be small and within the uncertainty of our RM values. Finally, the remarkably long duration from the co-addition of data significantly increases our ability to conduct this kind of analysis on a large number of pulsars that would otherwise not have the required S/N to robustly measure the RM.

As mentioned before, the data configuration of CHIME implies that we have a theoretical RMSF of ∼9 rad m$^{-2}$. Three of our new RMs fall within this range, notably PSR J1647+6608 with $RM_{obs}$ = 7(3) rad m$^{-2}$, PSR J1911+1347 with $RM_{obs}$ = −7(3) rad m$^{-2}$, and PSR J2340+08 with $RM_{obs}$ = −7(2) rad m$^{-2}$. Judging from their respective RM spectrum (see Figs C1–C3), the RM peak is clearly distinct from zero. This made us believe that these new RMs are reliable and not due to confusion with instrumental leakage.

## 5 DISCUSSION

We have updated 25 existing RM values of Northern hemisphere pulsars and measured 55 new RMs. These 80 pulsars are located in our full range of Right Ascension (RA) and $\delta$, spanning 1.5° ≤RA≤355.8° and −6.7° ≤ $\delta$ ≤ 83.2°. In terms of Galactic coordinates, which provide useful insight for studies looking at the Milky Way's magnetic field along longitudinal LOS, the pulsars lie within Galactic longitude of 20.6° ≤ $l$ ≤ 219.4° and Galactic latitude of −50.4° ≤ $b$ ≤ 54.2°. The range of updated RMs reported in this work lies between −295 rad m$^{-2}$ ≤$RM_{obs}$ ≤338 rad m$^{-2}$. The average $|RM_{obs}|$ in this study is roughly 70 rad m$^{-2}$. Combining the $DM_{obs}$ listed in Table A1, we can apply equation (3) to calculate the LOS parallel magnetic field strength, $<B_{||}>$ (last column of Table A1). According to Sun & Reich (2010), the strength of the regular halo magnetic field is about 2 μG, with which our results are largely consistent.

If we take into account the DM-derived distance of these pulsars as listed in the *ATNF* Pulsar Catalogue (based on the electron density model of Yao, Manchester & Wang 2017), we can locate the derived $<B_{||}>$ on a three-dimensional plot in Cartesian coordinates, as shown in Figs C4–C6. Note that most of the known pulsars do not have independent distance measurements (e.g. from parallax), and a majority of the pulsar distances are obtained from their DM, combined with a model of the free electron distribution, which is said to have uncertainty up to some 20 per cent. Keeping the caveat of the distance uncertainty in mind, we can still form an overview picture of the updated Faraday sky. In Fig. C4, we overlay the location of RM values from this work as well as all existing catalogue pulsar RMs with a simulation of the spiral arm structure of our Milky Way. It can be seen that most of our RMs fall within quadrants III and IV, and they also somewhat follow the arm structure. Compared to the recent LOFAR study by Sobey et al. (2019), we typically measure RMs farther out along the Galactic plane (up to ∼10 kpc) whereas LOFAR's sample is mostly concentrated near the Sun. This is likely due to less severe scattering and depolarization at the higher observing frequency of CHIME. In

terms of scale height ($z$), we cover a large range, detecting RMs up to $z$ ∼16 kpc. From our 80 updated RMs, we see a similar dichotomy already mentioned by Sobey et al. (2019) that $<B_{||}>$ values above the Galactic plane tend to be positive while those below the plane tend to be negative.

## 6 CONCLUSIONS

We present new measurements of RMs for northern radio pulsars, using commissioning data from CHIME/Pulsar. We report 55 new RMs and provide improved values and uncertainties for 25 pulsars with previously catalogued RMs. The wide bandwidth of CHIME has enabled our high RM precision. The observing frequency of 400–800 MHz is at a sweet spot for RM studies, low enough to take advantage of the wavelength squared dependency of RM and the steep spectrum of most pulsars but not so low as to be hindered by scattering and depolarization at high DM and RM. The high-cadence observations of CHIME also provide excellent S/N in our co-added data. We note that ionospheric RM corrections have not been applied in this work and it remains the biggest source of systematic uncertainty in our RMs.

The 80 updated RMs reported here cover a large region of the Milky Way, both deep in the Galactic plane and far out in the halo. The derived $<B_{||}>$ values are comparable to the average magnetic field strength of our Galaxy. Overall, this work improves our knowledge of the Faraday sky, with potential implications on future Galactic large-scale structure and ionospheric modelling studies.

## REFERENCES

Brentjens M. A., de Bruyn A. G., 2005, A&A, 441, 1217
Breton R. P. et al., 2013, ApJ, 769, 108
Brinkman C., Freire P. C. C., Rankin J., Stovall K., 2018, MNRAS, 474, 2012
CHIME/FRB Collaboration, 2018, ApJ, 863, 48
Gentile P. A. et al., 2018, ApJ, 862, 47
Hamilton P. A., Lyne A. G., 1987, MNRAS, 224, 1073
Han J. L., Manchester R. N., van Straten W., Demorest P., 2018, ApJS, 234, 11
Hankins T. H., Rankin J. M., 2010, AJ, 139, 168
Hobbs G. B., Edwards R. T., Manchester R. N., 2006, MNRAS, 369, 655

Hotan A. W., van Straten W., Manchester R. N., 2004, PASA, 21, 302
Johnston S., Hobbs G., Vigeland S., Kramer M., Weisberg J. M., Lyne A. G., 2005, MNRAS, 364, 1397
Lam M. T., Cordes J. M., Chatterjee S., Dolch T., 2015, ApJ, 801, 130
Lynch R. S. et al., 2013, ApJ, 763, 81
Manchester R. N., Hobbs G. B., Teoh A., Hobbs M., 2005, VizieR Online Data Catalog, 7245, 0
Mevius M., 2018a, Astrophysics Source Code Library, record ascl:1806.024
Mevius M., 2018b, in Heald G., McKean J., Pizzo R., eds, Low Frequency Radio Astronomy and the LOFAR Observatory, Astrophysics and Space Science Library, Vol. 426, Springer, Cham, p. 103
Mitra D., Wielebinski R., Kramer M., Jessner A., 2003, A&A, 398, 993
Morello V. et al., 2020, MNRAS, 493, 1165
Ng C., 2018, in Weltevrede P., Perera B. B. P., Preston L. L., Sanidas S., eds, Proc. IAU Symp. 337, Pulsar Astrophysics the Next Fifty Years, Cambridge University Press, Cambridge, UK, p. 179

Noutsos A., 2012, Space Sci. Rev., 166, 307
Noutsos A. et al., 2015, A&A, 576, A62
Phillips J. A., Wolszczan A., 1992, ApJ, 385, 273
Rand R. J., Lyne A. G., 1994, MNRAS, 268, 497
Sobey C. et al., 2019, MNRAS, 484, 3646
Sun X.-H., Reich W., 2010, Res. Astron. Astrophys., 10, 1287
Taylor G. B. et al., 2012, J. Astron. Instrum., 1, 1250004
Theureau G. et al., 2011, A&A, 525, A94
Tingay S. J. et al., 2013, PASA, 30, e007
Van Eck C. L. et al., 2011, ApJ, 728, 97
van Haarlem M. P. et al., 2013, A&A, 556, A2
van Straten W., Bailes M., 2011, PASA, 28, 1
van Straten W., Demorest P., Oslowski S., 2012, Astron. Res. Technol., 9, 237
Wayth R. B. et al., 2018, PASA, 35, 33
Yao J. M., Manchester R. N., Wang N., 2017, ApJ, 835, 29

## APPENDIX A: SUMMARY OF RESULTS

Summarized in Table A1 are the principal results of this study using the rmfit tool on co-added pulsar observations from CHIME/Pulsar. This table comprises 80 pulsars: 55 new RM results that have not been previously published and 25 updated RMs to the pulsar catalogue (version 1.61) with tighter bounds on the uncertainty.

Column 1 shows the pulsar name in B1950 or J2000 coordinate systems; the pulsars are listed in order of ascending RA. Columns 2–3 show the published RM results and uncertainties from the latest version of the *ATNF* pulsar catalogue (V 1.61) and column 4 includes a short hand of the corresponding literature reference in which the result was published. The full citation of these entries can be found in Table A2. Asterisks in columns 2–4 denote results that do not have a previously published RM result in the pulsar catalogue. Column 5 lists the MJD range of our CHIME/Pulsar data set and column 6 indicates the total length of fold mode observation in the co-added data. The S/N of the co-added profile can be found in column 7. The DM and the RM obtained from the co-added data are tabulated in columns 8–11. The uncertainty of our observed RM comes from the spread of the per-session RMs. When that is not available for the low S/N pulsars, uncertainty is taken from the RM spectrum Gaussian fit width calculated by rmfit. Our RMs do not include any ionospheric corrections. Columns 12–13 list the $<B_\parallel>$ and associated error derived from applying equation (3) to our DM and RM results.

**Table A1.** Summary of 80 co-added RMs obtained in this work. See Appendix A for a detailed description of each column.

| PSR | $RM_{cat}$ (rad m$^{-2}$) | ± (rad m$^{-2}$) | Ref | MJD | $Total_{fold}$ (h) | S/N | $DM_{obs}$ (pc cm$^{-3}$) | ± (pc cm$^{-3}$) | $RM_{obs}$ (rad m$^{-2}$) | ± (rad m$^{-2}$) | $<B_{||}>$ (µG) | ± (µG) |
|---|---|---|---|---|---|---|---|---|---|---|---|---|
| J0006+1834 | * | * | * | 58441–58740 | 10.7 | 76 | 12.4606 | 0.2000 | −20 | 3 | −2.008 | 0.041 |
| J0026+6320 | * | * | * | 58441–58467 | 1.2 | 82 | 245.1196 | 0.1000 | −294 | 2 | −1.483 | 0.002 |
| J0058+6125 | * | * | * | 58441–58742 | 38.0 | 94 | 128.6608 | 0.2000 | −212 | 2 | −2.032 | 0.006 |
| B0138+59 | −48.00 | 3.00 | hl87 | 58520–58711 | 38.4 | 1752 | 34.4630 | 0.4000 | −47.0 | 1.1 | −1.684 | 0.024 |
| B0144+59 | −19.00 | 5.00 | rl94 | 58321–58720 | 34.2 | 811 | 40.0862 | 0.0700 | −9.5 | 0.5 | −0.294 | 0.004 |
| B0154+61 | −29.00 | 7.00 | hl87 | 58520–58701 | 19.4 | 735 | 29.9132 | 9.0000 | −29 | 3 | −1.272 | 0.457 |
| J0201+7005 | * | * | * | 58634–58732 | 42.0 | 144 | 20.8587 | 0.5000 | −39 | 3 | −2.320 | 0.071 |
| J0324+5239 | * | * | * | 58441–58692 | 15.9 | 188 | 115.4211 | 0.1000 | −126 | 3 | −1.348 | 0.003 |
| B0331+45 | 5.60 | 0.09 | sbg+19 | 58398–58720 | 14.6 | 845 | 47.1117 | 0.1000 | −15.2 | 1.1 | −0.398 | 0.003 |
| B0339+53 | −84.00 | 20.00 | mwkj03 | 58351–58715 | 17.6 | 606 | 68.0324 | 0.7000 | −69.7 | 1.5 | −1.264 | 0.016 |
| J0340+4130 | * | * | * | 58520–58744 | 81.9 | 361 | 49.5823 | 0.0003 | 56.1 | 0.7 | 1.395 | 0.002 |
| B0355+54 | 79.00 | 4.00 | hl87 | 58318–58711 | 41.0 | 6561 | 57.1223 | 0.0600 | 81.5 | 0.3 | 1.758 | 0.003 |
| J0426+4933 | * | * | * | 58500–58691 | 6.5 | 346 | 84.1850 | 0.3000 | −169 | 7 | −2.485 | 0.012 |
| J0453+1559 | * | * | * | 58439–58688 | 7.6 | 103 | 30.2880 | 0.0100 | −35 | 2 | −1.435 | 0.018 |
| J0517+2212 | −16.00 | 0.00 | bfrs18 | 58439–58714 | 10.9 | 1030 | 18.6769 | 0.0800 | −20.2 | 1.6 | −1.338 | 0.009 |
| J0538+2817 | −7.00 | 12.00 | mwkj03 | 58321–58709 | 8.9 | 886 | 39.8826 | 0.0500 | 39 | 3 | 1.220 | 0.002 |
| J0540+3207 | * | * | * | 58520–58701 | 19.2 | 370 | 61.9038 | 0.2000 | 13.7 | 1.8 | 0.273 | 0.004 |
| J0546+2441 | 8.00 | 6.10 | hmvd18 | 58320–58735 | 12.6 | 294 | 73.0922 | 1.0000 | 24 | 3 | 0.407 | 0.008 |
| J0555+3948 | * | * | * | 58520–58744 | 19.6 | 183 | 36.7105 | 0.4000 | 9 | 3 | 0.325 | 0.015 |
| J0613+3731 | * | * | * | 58518–58720 | 5.5 | 178 | 18.7556 | 0.2000 | 16 | 2 | 1.082 | 0.017 |
| J0614+83 | * | * | * | 58702–58737 | 19.2 | 45 | 43.8689 | 0.4000 | −13 | 3 | −0.385 | 0.090 |
| J0627+0649 | * | * | * | 58456–58692 | 2.9 | 113 | 86.5563 | 0.1000 | 179 | 3 | 2.555 | 0.004 |
| J0646+0905 | * | * | * | 58519–58640 | 8.7 | 190 | 148.8859 | 0.3000 | −149 | 2 | −1.239 | 0.003 |
| J0711+0931 | * | * | * | 58520–58744 | 8.5 | 127 | 46.0848 | 0.4000 | 62.8 | 1.1 | 1.684 | 0.018 |
| J0740+6620 | * | * | * | 58517–58731 | 78.5 | 385 | 14.9626 | 0.0002 | −36 | 2 | −3.040 | 0.010 |
| J0751+1807 | 9.00 | 14.00 | hmvd18 | 58321–58701 | 11.2 | 149 | 30.2438 | 0.0010 | 44 | 3 | 1.803 | 0.006 |
| J0815+0939 | 53.10 | 5.00 | hmvd18 | 58321–58715 | 10.0 | 127 | 53.0660 | 0.2000 | 54 | 2 | 1.275 | 0.009 |
| J0843+0719 | * | * | * | 58321–58715 | 9.4 | 48 | 33.5864 | 0.5000 | 40 | 4 | 1.506 | 0.037 |
| J1434+7257 | * | * | * | 58516–58700 | 34.5 | 267 | 12.5997 | 0.0100 | −9.7 | 1.2 | −0.951 | 0.017 |
| J1518+4904 | −15.60 | 3.70 | hmvd18 | 58441–58733 | 17.6 | 2714 | 11.6062 | 0.0100 | −11.9 | 1.3 | −1.271 | 0.013 |
| J1538+2345 | * | * | * | 58520–58741 | 9.7 | 141 | 14.4737 | 1.0000 | 11.5 | 1.1 | 1.020 | 0.093 |
| J1544+4937 | * | * | * | 58520–58742 | 54.5 | 248 | 23.2280 | 0.0008 | 9.8 | 1.9 | 0.523 | 0.010 |
| B1612+07 | 40.00 | 4.00 | hl87 | 58329–58715 | 11.9 | 440 | 21.2426 | 0.4000 | 28 | 3 | 1.677 | 0.042 |
| B1639+36A | * | * | * | 58359–58693 | 25.3 | 112 | 30.4310 | 0.0040 | 13 | 3 | 0.532 | 0.012 |
| J1647+6608 | * | * | * | 58501–58742 | 22.5 | 107 | 22.7981 | 0.6000 | 7 | 3 | 0.411 | 0.017 |
| J1710+4923 | * | * | * | 58542–58721 | 13.2 | 193 | 7.0826 | 0.0010 | 12 | 2 | 2.117 | 0.165 |
| J1736+05 | * | * | * | 58450–58718 | 10.0 | 54 | 38.6724 | 0.3000 | 44 | 3 | 1.417 | 0.027 |
| J1738+0333 | 36 | 9 | gmd+18 | 58515–58744 | 35.3 | 70 | 33.7652 | 0.0040 | 33 | 3 | 1.235 | 0.027 |
| B1802+03 | 38.90 | 3.70 | hmvd18 | 58328–58711 | 39.2 | 285 | 80.8294 | 0.0800 | 42 | 2 | 0.644 | 0.005 |
| J1821+0155 | * | * | * | 58683–58719 | 4.7 | 56 | 51.7499 | 0.0100 | 110 | 3 | 2.638 | 0.014 |

**Table A1** – *continued*

| PSR | RM$_{cat}$ (rad m$^{-2}$) | ± (rad m$^{-2}$) | Ref | MJD | Total$_{fold}$ (h) | S/N | DM$_{obs}$ (pc cm$^{-3}$) | ± (pc cm$^{-3}$) | RM$_{obs}$ (rad m$^{-2}$) | ± (rad m$^{-2}$) | $<B_{||}>$ (µG) | ± (µG) |
|---|---|---|---|---|---|---|---|---|---|---|---|---|
| J1834+10 | * | * | * | 58721–58739 | 2.0 | 23 | 78.0350 | 0.7000 | 97.0 | 1.7 | 1.533 | 0.041 |
| J1900+30 | * | * | * | 58715–58739 | 3.9 | 128 | 71.7592 | 0.2000 | 121 | 2 | 2.094 | 0.011 |
| J1911+1347 | * | * | * | 58472–58742 | 24.6 | 87 | 30.9806 | 0.0004 | −7 | 3 | −0.282 | 0.011 |
| J1918−0642 | * | * | * | 58500–58742 | 31.7 | 102 | 26.5890 | 0.0030 | −57 | 3 | −2.648 | 0.207 |
| B1926+18 | * | * | * | 58365–58660 | 3.0 | 49 | 111.5379 | 0.4000 | 174 | 2 | 1.931 | 0.012 |
| J1946+2535 | * | * | * | 58443–58708 | 2.0 | 39 | 248.4199 | 0.1000 | 57 | 3 | 0.293 | 0.015 |
| J1946+2611 | −88.70 | 1.70 | hmvd18 | 58461–58662 | 3.3 | 93 | 165.3295 | 0.1000 | −83.9 | 1.3 | −0.626 | 0.002 |
| B1952+29 | −18.00 | 3.00 | hl87 | 58501–58662 | 6.3 | 530 | 7.8782 | 0.1000 | −16 | 2 | −2.567 | 0.041 |
| B2002+31 | 30.00 | 6.00 | hl87 | 58520–58701 | 32.4 | 1451 | 234.5535 | 0.8000 | 31.5 | 0.8 | 0.166 | 0.001 |
| J2010+2845 | * | * | * | 58450–58705 | 5.2 | 146 | 112.3273 | 0.2000 | −233 | 3 | −2.560 | 0.007 |
| J2011+3331 | * | * | * | 58521–58664 | 13.4 | 172 | 298.3448 | 0.3000 | 235.6 | 0.5 | 0.973 | 0.002 |
| J2013+3058 | * | * | * | 58441–58650 | 6.6 | 174 | 148.6652 | 0.1000 | −145 | 3 | −1.204 | 0.007 |
| J2016+1948 | * | * | * | 58451–58661 | 7.2 | 131 | 33.7492 | 0.2000 | −121 | 4 | −4.419 | 0.033 |
| J2017+5906 | * | * | * | 58509–58636 | 10.6 | 174 | 59.9378 | 0.1000 | 33 | 3 | 0.696 | 0.005 |
| J2019+2425 | −71 | 4 | gmd+18 | 58521–58677 | 7.8 | 189 | 17.1985 | 0.0010 | −67.6 | 0.6 | −4.843 | 0.006 |
| B2025+21 | * | * | * | 58448–58664 | 8.1 | 64 | 96.9408 | 0.1000 | −210 | 2 | −2.680 | 0.007 |
| J2027+4557 | * | * | * | 58447–58717 | 8.5 | 368 | 229.4552 | 0.4000 | 337 | 3 | 1.815 | 0.004 |
| J2040+1657 | * | * | * | 58445–58737 | 5.1 | 72 | 50.2550 | 0.3000 | −98 | 2 | −2.413 | 0.021 |
| J2045+0912 | −89.50 | 3.90 | hmvd18 | 58445–58737 | 21.7 | 338 | 31.3267 | 0.1000 | −84.7 | 1.9 | −3.337 | 0.015 |
| J2047+5029 | * | * | * | 58487–58701 | 6.7 | 118 | 107.8448 | 0.1000 | −121 | 4 | −1.394 | 0.004 |
| B2053+36 | −68.00 | 4.00 | hl87 | 58440–58700 | 43.2 | 3082 | 97.3875 | 0.0800 | −63.4 | 0.3 | −0.802 | 0.001 |
| J2102+38 | * | * | * | 58440–58701 | 28.0 | 255 | 86.0513 | 0.4000 | −74 | 2 | −1.062 | 0.007 |
| B2122+13 | −48.30 | 3.60 | hr10 | 58440–58711 | 9.9 | 242 | 30.1597 | 0.2000 | −43 | 3 | −1.797 | 0.016 |
| J2138+4911 | * | * | * | 58440–58693 | 7.3 | 441 | 168.2636 | 0.2000 | −143 | 3 | −1.052 | 0.002 |
| J2139+00 | * | * | * | 58445–58693 | 27.6 | 353 | 31.2913 | 0.1000 | 11 | 2 | 0.439 | 0.007 |
| B2148+52 | −44.00 | 11.00 | mwkj03 | 58443–58715 | 57.5 | 1564 | 149.0138 | 0.1000 | −19.0 | 0.8 | −0.157 | 0.001 |
| J2208+4056 | * | * | * | 58452–58722 | 13.2 | 76 | 11.7588 | 0.2000 | −40 | 3 | −4.316 | 0.106 |
| J2208+5500 | * | * | * | 58439–58693 | 5.1 | 234 | 104.5698 | 0.3000 | −87 | 3 | −1.027 | 0.007 |
| J2216+5759 | * | * | * | 58521–58722 | 12.7 | 184 | 167.3322 | 0.1000 | −10.9 | 1.7 | −0.081 | 0.001 |
| J2217+5733 | * | * | * | 58456–58718 | 16.0 | 491 | 130.6711 | 0.4000 | −90 | 3 | −0.085 | 0.004 |
| J2227+30 | * | * | * | 58456–58605 | 5.1 | 589 | 19.9559 | 0.3000 | −58.3 | 1.9 | −3.612 | 0.068 |
| J2229+6114 | * | * | * | 58451–58664 | 16.1 | 484 | 204.9635 | 0.0200 | −187 | 3 | −1.129 | 0.001 |
| J2234+2114 | −91.50 | 2.50 | hmvd18 | 58652–58722 | 3.9 | 191 | 34.7371 | 0.5000 | −93.7 | 1.8 | −3.329 | 0.060 |
| J2240+5832 | 24.00 | 4.00 | tpc+11 | 58455–58701 | 17.8 | 357 | 263.4647 | 0.0500 | 17.1 | 1.1 | 0.080 | 0.001 |
| J2243+1518 | * | * | * | 58440–58722 | 10.0 | 66 | 39.6448 | 0.2000 | −35.5 | 0.5 | −1.120 | 0.020 |
| J2302+4442 | * | * | * | 58450–58709 | 45.0 | 269 | 13.7196 | 0.0005 | 19.1 | 1.6 | 1.715 | 0.004 |
| J2310+6706 | * | * | * | 58440–58651 | 3.7 | 29 | 98.5726 | 0.7000 | −16 | 2 | −0.204 | 0.008 |
| J2319+6411 | * | * | * | 58519–58731 | 9.8 | 1393 | 245.9455 | 0.0800 | −48.8 | 1.2 | −0.244 | 0.001 |
| J2340+08 | * | * | * | 58519–58701 | 8.8 | 118 | 23.9234 | 0.1000 | −7 | 2 | −0.388 | 0.022 |
| J2343+6221 | * | * | * | 58652–58701 | 65.7 | 303 | 155.8648 | 0.6000 | −44.9 | 0.9 | −0.356 | 0.002 |

**Table A2.** Summary of the references for the catalogue RMs listed in Table A1.

| Shorthand | Reference | (Lowest) Centre frequency (MHz) | Ionospheric RM corrected |
|---|---|---|---|
| bfrs18 | Brinkman et al. (2018) | 327 | N |
| gmd+18 | Gentile et al. (2018) | 1400 | N |
| hl87 | Hamilton & Lyne (1987) | 408 | Y |
| hmvd18 | Han et al. (2018) | 774 | Y |
| hr10 | Hankins & Rankin (2010) | 50 | N |
| lbr+13 | Lynch et al. (2013) | 350/820 | N |
| mwkj03 | Mitra et al. (2003) | 1400 | N |
| rl94 | Rand & Lyne (1994) | 1400 | N |
| sbg+19 | Sobey et al. (2019) | 110 | Y |
| tpc+11 | Theureau et al. (2011) | 1100 | N |

## APPENDIX B: SUMMARY OF FARADAY SPECTRA OBSERVATIONS

Figs C1 through C3 show the individual Faraday spectra of the 80 RM results presented in Table A1. The *x*-axes show the appropriate RM range that incorporates the peak RM values. The *y*-axes show normalized polarized flux in arbitrary units as our data are uncalibrated in polarization. Peaks centred at $0\,\mathrm{rad\,m^{-2}}$ and symmetric peaks about $0\,\mathrm{rad\,m^{-2}}$ are due to instrumental leakage discussed in Section 2. The $\mathrm{RM_{obs}}$ is shown as a vertical dashed line and its corresponding uncertainty is represented by vertical solid lines, although in almost all cases the uncertainty range is too small to visually separate the three lines. When available, the catalogue RM ($\mathrm{RM_{cat}}$) is represented by a vertical red dash–dot line and its corresponding uncertainty region is marked by the shaded hatch.

## APPENDIX C: PULSARS WITH NO DETECTED RM

In addition to the 80 RMs reported in this work, a further 54 pulsars were studied although no RM was detected in them. Instrumental leakage dominated 30 pulsars, namely PSRs J0023+0923, J0051+0423, J0243+6027, J0329+1654, J0458–0505, J0609+2130, J0611+1436, J0621+0336, J0630–0046, J0647+0913, J1125+7819, J1327–0755, J1501–0046, J1628+4406, B1740–13, J1744–1610, J1745–0129, J1802+0128, J1807+0756, B1810+02, J1820–0509, B1831–00, J2018+3431, J2048+2255, J2123+5434, J2206+6151, J2228+6447, J2325–0530, J2333+6145, and J2352+65. A further 24 pulsars likely have intrinsically weak polarization, namely PSRs J0103+54, J0139+5621, J0332+79, J0337+1715, J0645+80, J0652–0142, B1740–03, J1819–1318, J1842+0638, J1843+2024, J1846–0749, J1846–07492, J1848+0826, B1904+12, B1906+09, J1925+19, J1931+30, B1933+17, J1954+4357, B1957+20, J2002+30, J2013–0649, J2015+2524, and J2030+55.
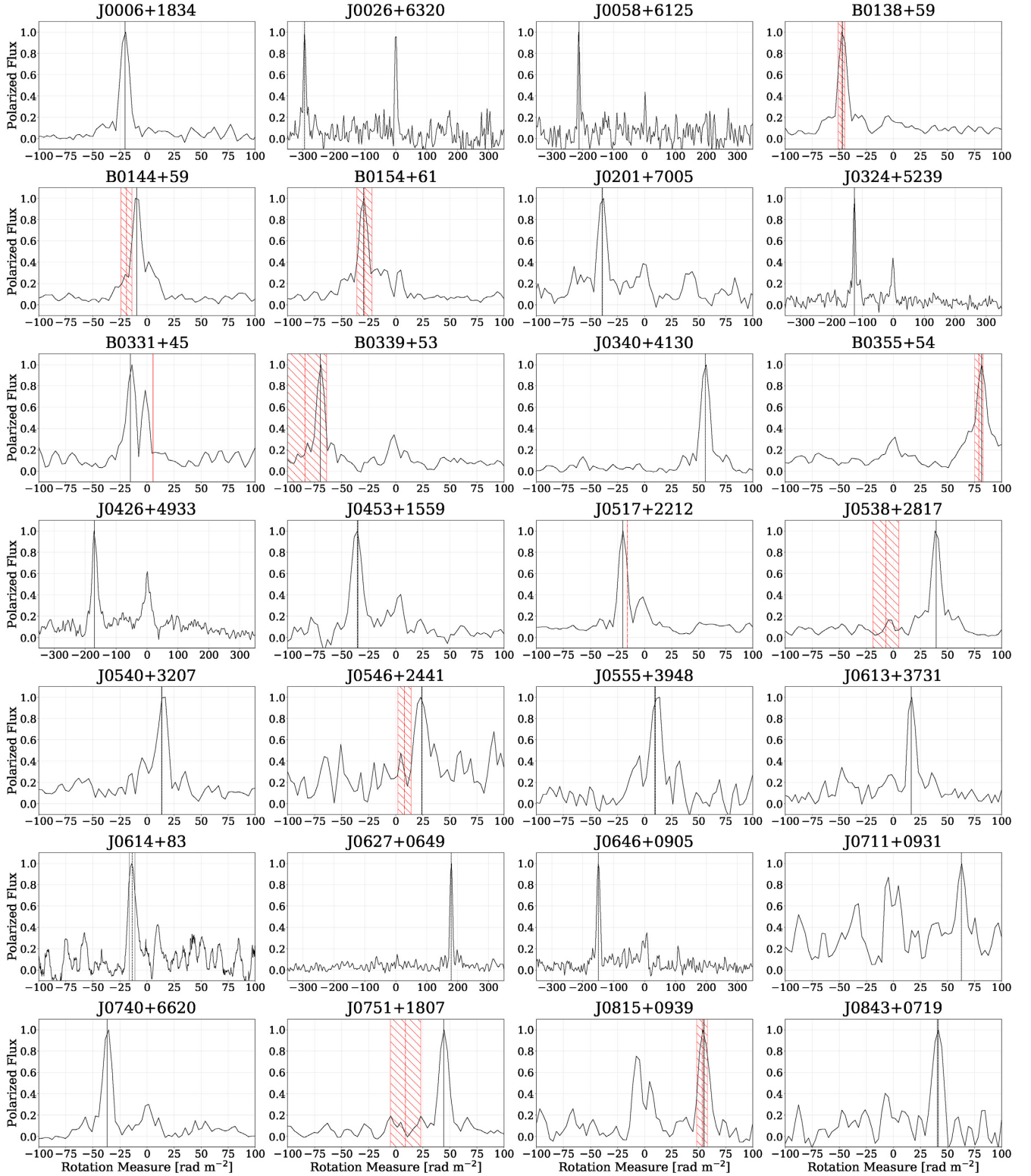
**Figure C1.** Faraday spectra of the 80 pulsars in this work. Refer to text for further description of the figures.
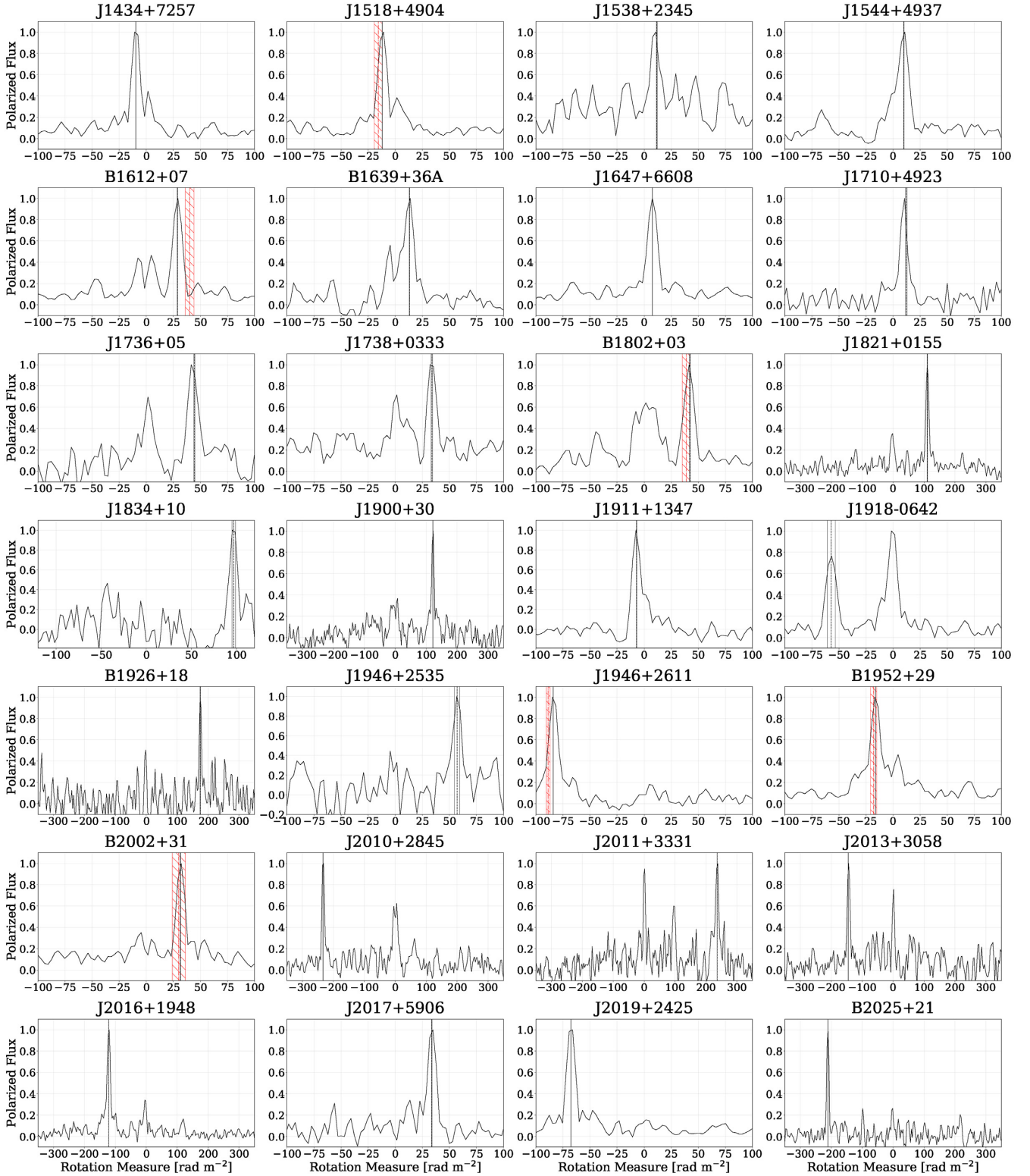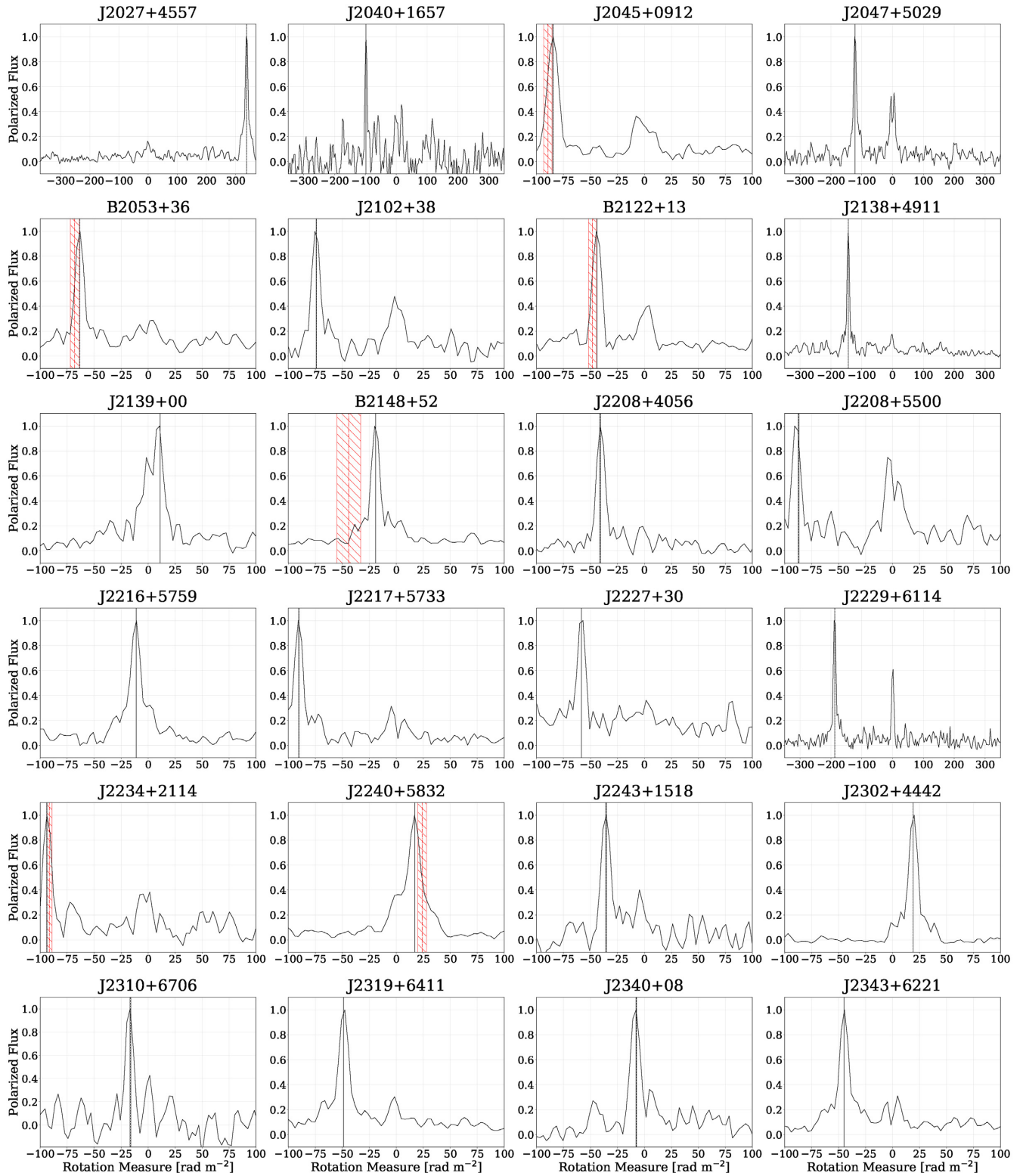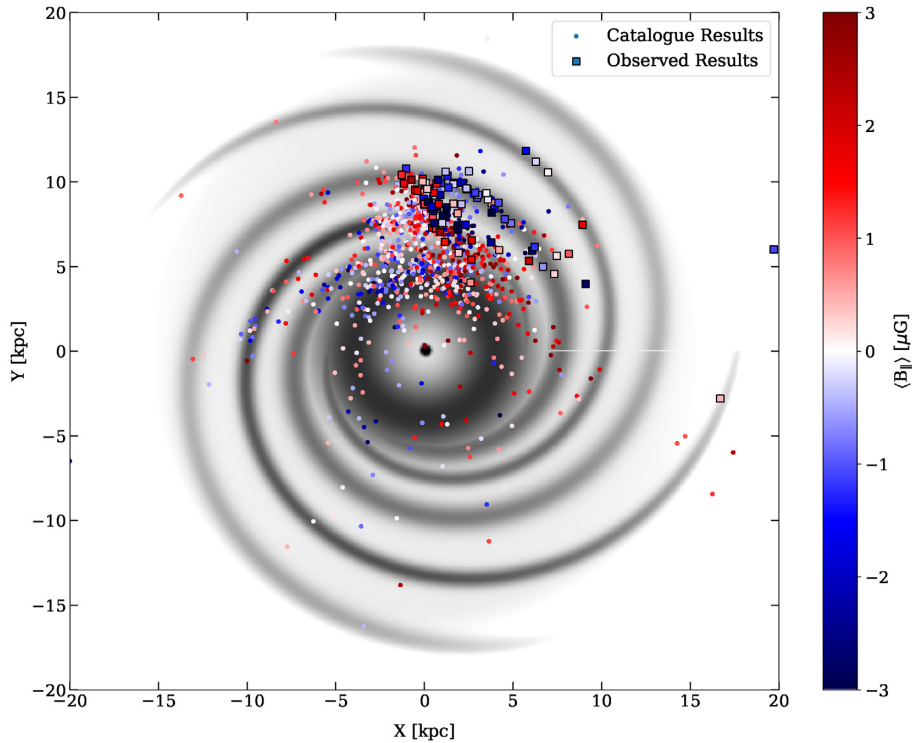
**Figure C2-** *Continued*

**Figure C3-** *Continued*

**Figure C4.** X–Y plane of the Milky Way, where the Sun is defined to be at (X,Y) = (0,8.3) kpc and the Galactic Centre at (X,Y) = (0,0) kpc. The pulsars with catalogue RM values are shown as circles, whereas the 80 updated RMs from this work are represented by squares. The colour scale of these symbols gives the $<B_{||}>$. Pulsars with $z > |16|$ kpc are not shown for clarity of the local distribution. The electron density in the plane of the Galaxy used in the YMW16 model is also shown in grey-scale.
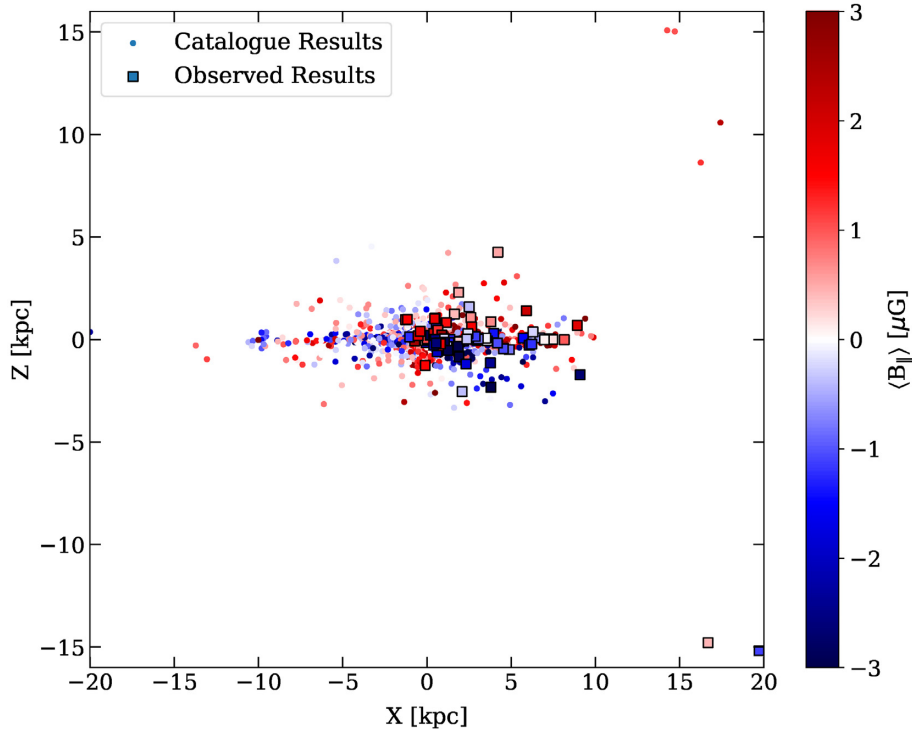


**Figure C5.** X–Z plane of the Milky Way, with the same plotting organization as Fig. C4.
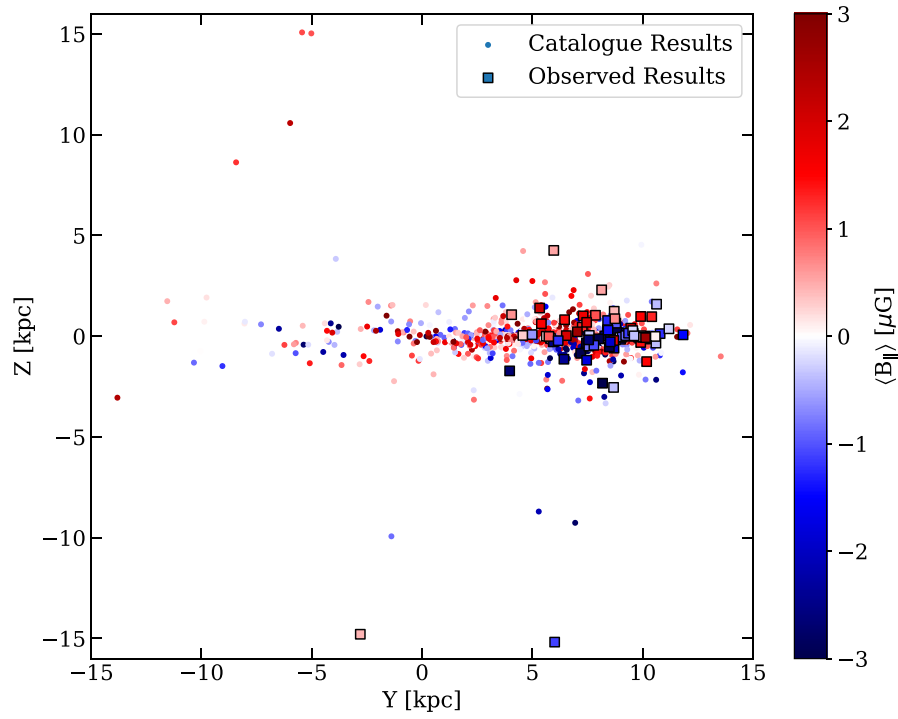
**Figure C6.** Y–Z plane of the Milky Way, with the same plotting organization as Fig. C4.

This paper has been typeset from a TₑX/LᴬTₑX file prepared by the author.